Beyond-Bandwidth Electrical Pulse Modulation of a TO-Can Packaged VCSEL for 10 Gbit/s Injection-Locked NRZ-to-RZ Transmission

Chia-Chi Lin, Yu-Chieh Chi, Hao-Chung Kuo, *Senior Member, IEEE*, Peng-Chun Peng, *Member, IEEE*, Connie J. Chang-Hasnain, *Fellow, IEEE*, and Gong-Ru Lin, *Senior Member, IEEE*

***Abstract*—The parametric characterization of a nonreturn-to-zero (NRZ) to return-to-zero (RZ) data format converter based on the external optical NRZ injection of a TO-46-can packaged vertical-cavity surface-emitting laser (VCSEL) directly modulated by a 10 GHz electrical pulse is demonstrated. The electrical-pulse modulation induced gain switching of the VCSEL is initiated under external optical NRZ data injection that increases the relaxation oscillation frequency of the homemade VCSEL from 2.2 to 7.4 GHz, thereby enabling its electrical modulation bandwidth up to 10 GHz. The external NRZ injection reduces the lasing threshold and enlarges the modulation depth of the VCSEL so that the converted RZ data pulsewidth can be shortened to 27 ps with a slightly increased peak-to-peak negative frequency chirp of 4.3 GHz (corresponding to a chirp parameter of 122 MHz/ps). The chirp and bit error rate (BER) display strong correlations with the injection power and the biased current of the VCSEL. With external injection, the receiving power required for achieving a BER below 10^{-9} at 10 Gbit/s is -19.5 dBm, and a power penalty of 16 dB is observed when the dc bias of the electrical-pulse modulated VCSEL is decreased by only 10% from the threshold condition.**

***Index Terms*—Chirp parameter, data format convertor, injection-locked, return-to-zero (RZ), vertical-cavity surface-emitting laser (VCSEL).**

I. Introduction

An all-optical return-to-zero (RZ) data generator is a necessary element of the future high-bit-rate optical time-division-multiplexing communication system. Typically, the RZ-pulsed data format is better for long-haul transmission at a bit rate of 10 Gbit/s than the conventional nonreturn-to-zero (NRZ) data format, as it is relatively insensitive to the optical nonlinearity and the polarization mode dispersion in single-mode fibers after appropriate compensation [1], [2]. Numerous scenarios have been proposed to demonstrate RZ generation and NRZ-to-RZ conversion, with simplified all-optical schemes persistently emerging during the past decade. By using a directly gain-modulated and single- (or dual-) wavelength injection-locked Fabry–Perot laser diode (FPLD), the NRZ-to-RZ data format conversion can only be performed at low bit rates (<3 Gbit/s) [3], [4]. Some of the 10 Gbit/s "all-optical" NRZ-to-RZ converters have been demonstrated by using semiconductor optical amplifiers (SOAs) and/or loop mirrors under a self- or cross-phase modulation scheme [5]–[7]. Alternatively, optoelectronic oscillators [8], the periodically poled $LiNbO_3$ (PPLN) waveguide with cascaded second-order nonlinearity [9], and the SOA-based bidirectional four-wave mixing techniques [10] were shown to increase the bit rates for all-optical conversion up to 10–40 Gbit/s. Even though these high-performance techniques were addressed to implement NRZ-to-RZ conversion, the relatively complicated and expensive setups still restrict their practical applications. Not long ago, the external injection seeding of a gain-switched FPLD was reported to facilitate optical pulse generation up to 20 GHz [11]. However, this technique also suffers from substantial mode beating noise that restricts its long-term stability and suitability for high-bit-rate communication.

Recently, the single-chip vertical-cavity surface-emitting laser (VCSEL) has shown its great potential for high-speed data transmission up to 22 Gbit/s [12], and the transmitter optical subassembly (TOSA) packaged VCSEL with DCF modules was shown to enable 10.3 Gbit/s transmission at 1.55 μm [13]. The reference work indeed presents a state-of-the-art performance of the VCSEL. In addition, the modulation bandwidth of the VCSEL can further be enhanced to 38 [14] and 40 GHz [15] by means of external optical injection. A similar work using VCSEL-to-VCSEL injection for 10 Gbit/s NRZ transmission with a pattern length of $2^7 - 1$ [16] was also reported. Apart from dual-mode switching [17], polarization bistability [18], [19], and modulated injection locking techniques [20], there are really few demonstrations reported of an RZ data stream generated from a VCSEL. Up to now, most reports focused on characterizing the modulation bandwidth and the transmission data rate of the VCSEL chip, with or without the specific laser package. In contrast to the frequency bandwidth of a VCSEL

Manuscript received July 12, 2010; revised September 23, 2010, November 13, 2010, December 21, 2010; accepted December 22, 2010. Date of publication December 30, 2010; date of current version March 02, 2011. This work was supported in part by the National Science Council, Taiwan, and the Excellent Research Projects of National Taiwan University, Taiwan, under Grants NSC 98-2221-E-002-023-MY3, NSC 98-2623-E-002-002-ET, and NSC 98-2622-E-002-023-CC3.

C.-C. Lin, Y.-C. Chi and G.-R. Lin are with the Graduate Institute of Photonics and Optoelectronics, and the Department of Electrical Engineering, National Taiwan University, Taipei 10617, Taiwan (e-mail: grlin@ntu.edu.tw).

H.-C. Kuo is with the Department of Photonics, National Chiao Tung University, Hsinchu 300, Taiwan.

P.-C. Peng is with the Department of Electro-Optical Engineering, National Taipei University of Technology, Taipei 10608, Taiwan.

C. J. Chang-Hasnain is with the Department of EECS, University of California—Berkeley, CA 94720-1776 USA.

Color versions of one or more of the figures in this paper are available online at http://ieeexplore.ieee.org.

Digital Object Identifier 10.1109/JLT.2010.2103551

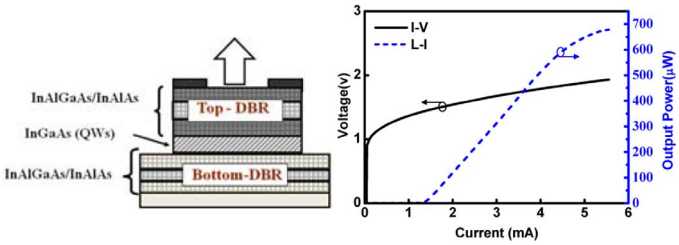

Fig. 1. Structural diagram of the VCSEL (left) and its characteristics (right).

chip, frequency bandwidth of a commercially available VCSEL with a transistor outline can (TO-46-can) package is further reduced to <2.488 Gbit/s (ITU-T defined OC-48 transmission rate) by the use of the bonding wire from lead to submount and from lead to VCSEL anode in common TO-can module because of the effects of the parasitic capacitance and inductor in the TO-can package. Beyond 4 GHz, optical cross-gain modulation at 10 Gbit/s is rather difficult to implement in the TO-46-can packaged VCSEL. Even though the injection locking technique has been used to improve the direct modulation bandwidth of the VCSEL [21], the maximum bit rate of a TO-46-can packaged VCSEL is still limited to below 2.5 Gbit/s [20]. While the multifunctional operation (ultrawideband monocycle generation, pseudo-RZ data format conversion, and NRZ data clock recovery) of a specific VCSEL under optical injection locking has been demonstrated at 10 Gbit/s with an assistant filter [22], the injection-locked VCSEL used with an optimized high-speed design and its modulation bandwidth are not limited by the package. Despite the considerable difficulties facing the application of the TO-46-can packaged VCSEL, such as a finite-modulation bandwidth and an extremely small detuning bias range, the 10-Gbit/s NRZ-to-RZ conversion of a TO-46-can packaged VCSEL via direct modulation and external injection is still a simplified and practical carrier module for all-optical RZ networks.

In this paper, we propose a 10-Gbit/s all-optical NRZ-to-RZ convertor by injection locking in the electrical-pulse driven TO-46-can VCSEL biased at unlasing condition that induces gain switching as well as real RZ data format conversion under the external optical NRZ injection. In particular, the investigation of the RZ transmission performance is different from that of the pseudo-RZ format with its ON bit located at the rising and falling edges of the NRZ data bit that has been studied in the previous studies. This technique overcomes the inherent limitations on the direct modulation bandwidth of a TO-46-can packaged VCSEL. The eye diagram, pulse extinction ratio (ER), frequency chirp, and bit error rate (BER) performances of the generated RZ data stream at 10 Gbit/s are parametrically analyzed. In addition, we discuss the optimized ER of the converted RZ data for improving the transmission performance by tuning the dc-biased current and the external injection power of the gain-switched VCSEL.

II. Experimental Setup

The structure diagram and the characteristic transfer function of the homemade 1550 nm VCSEL used in the RZ data generator are shown in Fig. 1.

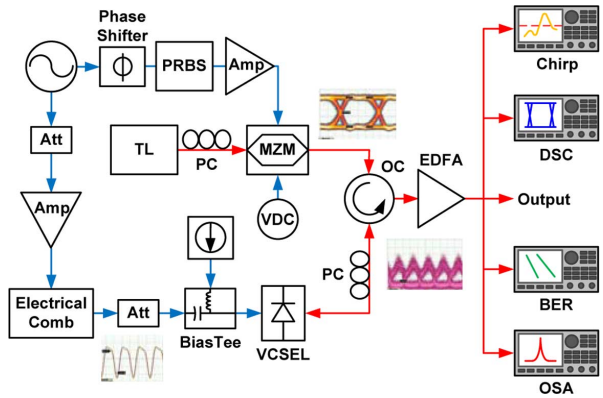

Fig. 2. VCSEL based 10-Gbit/s NRZ-to-RZ convertor. Amp: microwave amplifier; MZM: Mach–Zehnder modulator; OC: optical circulator; PC: polarization controller; TL: tunable laser; and Att: attenuator.

The homemade VCSEL was fabricated with a one-step low-pressure metal-organic chemical vapor deposition technique [23], [24]. The active region was formed by seven pairs of monolithic strain-compensated InGaAs quantum wells (QWs). These were sandwiched between undoped InAlGaAs–InA1As distributed Bragg reflectors on InP wafers. Such a VCSEL exhibits a threshold current of 1.3 mA and a slope efficiency of 0.07 mW/mA, which is packaged in a TO-46-can pig-tailed with a single-mode fiber (Corning SMF-28) for subsequent experiments. Fig. 2 illustrates the experimental setup of a VCSEL based all-optical 10-Gbit/s RZ data generator in which the gain switching RZ carrier is initiated by externally NRZ injection locking the electrical-pulse modulated VCSEL at 10 GHz. The VCSEL is biased at 1.2–1.4 mA, and then, synchronously modulated with the attenuated electrical pulse. The electrical pulse, with a width of 30 ps, is generated using an amplified 10 GHz microwave signal from a frequency synthesizer (Agilent E8257C) at an output power of −10 dBm in connection with a driver amplifier (with a power gain of 30 dB). During operation, the peak voltage of the electrical pulse is maintained below the breakdown condition of the VCSEL. Originally, the output power of the electrical pulse generator is about 10 dBm. A constant power attenuator (−9 dB) is applied to protect the VCSEL from overdriven damage. By taking the source impedance as $Z_0 = 50\ \Omega$ and the effect load resistance of the VCSEL as $Z_R = 20\ \Omega$, the load reflection coefficient $\Gamma = \sqrt{[(Z_o - Z_R)^2 + J^2]/[(Z_o + Z_R)^2 + J^2]}$ is determined to be 0.43 if the imaginary impedance J is ignored for simplicity. The equivalent biased current contributed by the modulated electrical pulse can be estimated using $i_p = \sqrt{\alpha_{\text{att}}\Gamma V_p/Z_R}$, where α_{att} denotes the attenuation loss. As a result, the i_p is determined to be 6.3 mA and the maximum of the total current applied to the electrical-pulse modulated VCSEL without external injection is $i_{\text{total}} = i_{\text{dc}} + i_{\text{p}} = 1.4 + 6.3 = 7.7$ mA.

Using an amplified pseudorandom bit sequence (PRBS) data generator (Hewlett Packard, HP70843B) with a pattern length of $2^{23} - 1$ at 10 Gbit/s, the optical NRZ data stream with an average power of −15 dBm was obtained by externally encoding a tunable laser (ANDO, AQ4321) at a wavelength of 1529.5 nm through a Mach–Zehnder intensity modulator (MZM) linearly

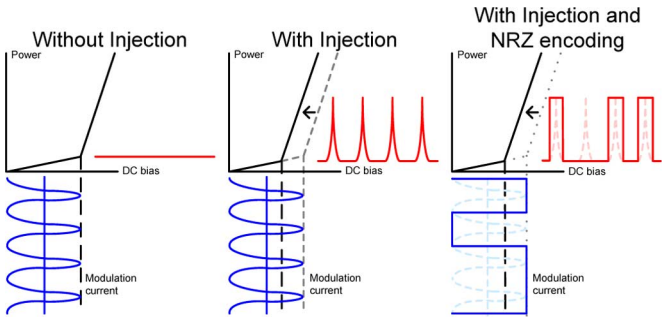

Fig. 3. Operating principle of the electrical-pulse modulated VCSEL under an optical injection locking for NRZ-to-RZ conversion.

biased at $V_{\rm drive} = 4.8$ V. The VCSEL temperature was controlled at 25 °C, with a fluctuation of <0.1°C, to prevent the wavelength from drifting from its lasing mode, thus ensuring that the injection locking wavelength was precisely within the locking range of the VCSEL. The injection locking range of the VCSEL was about 0.05 nm, which is comparable to those previously reported [22]. Consequently, the lasing threshold of the VCSEL was effectively reduced by the incoming high-level NRZ injection, while the gain-switched VCSEL was initiated to implement RZ data generation at 10 Gbit/s.

III. Results and Discussion

Under electrical pulse modulation and external injection, the operating principle of the gain-switched VCSEL for NRZ-to-RZ conversion at nearly threshold condition is illustrated in Fig. 3. The left and middle parts of Fig. 3 show, respectively, the electrical-pulse modulated VCSEL output without and with external injection (which causes an additional threshold reduction). With the injected optical NRZ data stream, the gain switching of the VCSEL is initiated to provide an RZ data stream output within 1 bit period of the incoming NRZ data. Note that the RZ data format in our case is different from the pseudo-RZ one discussed in the previous study [22]. The obtained RZ data format returns to zero between bits. In this format, the "1" level results from the presence of light for half a bit period, and the "0" level turns OFF the light for the rest of the period.

Subsequently, the frequency response is characterized for the original relaxation frequency of the TO-46-can packaged VCSEL with and without external injection, as shown in Fig. 4 . The typical relaxation oscillation frequency and modulation bandwidth of the free-running VCSEL under direct modulation is 2 and 2.6 GHz, as shown in Fig. 4. With the external injection of −5 dBm, the relaxation oscillation frequency of the homemade VCSEL can be increased from 2 to 7.3 GHz. The injection only causes a finite increase of the analog modulation bandwidth from 2.6 to 8 GHz since the cutoff frequency is still limited by the TO-46-can package and other parasitic components. To facilitate the RZ operation of the VCSEL up to 10 Gbit/s, both electrical pulse modulation and external optical injection have been employed in this paper. The electrical pulse modulation and the external injection technique overcome the inherent limitation on the direct modulation bandwidth of the laser diode packaged with a TO-can. However, it is unable

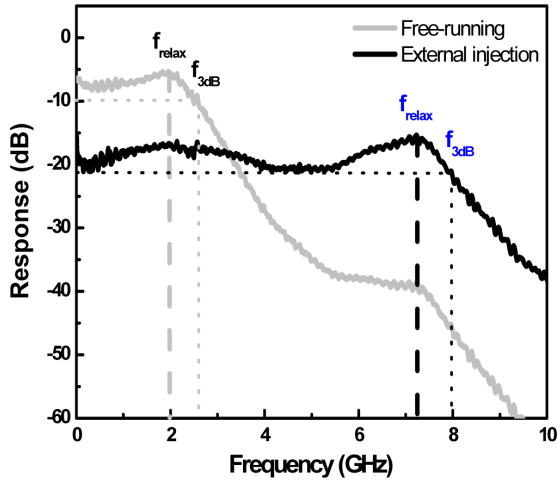

Fig. 4. Frequency response of the VCSEL without (gray curve) and with (black curve) external injection.

to compare the modulation bandwidth performance of the VCSEL operated in direct modulation mode (with sinusoidal waveform output) with that of the VCSEL operated in RZ generation mode (with pulsed carrier output). The output frequency spectrum of a directly modulated VCSEL exhibits only a single-frequency component, whereas that of the electrical-pulse modulated VCSEL provides a spectrum containing a set of frequency components. Nevertheless, the spectra of the VCSEL operated under different conditions have been obtained using a microwave spectrum analyzer, and the differences are addressed in more detail in a later section.

To elucidate the enhanced frequency response of the VCSEL based RZ generator under an injection locking condition, we must clarify the effects of externally injected photons and a biased current on the relaxation oscillation frequency of the VCSEL. According to the state-of-the-art model established in previous tutorial study [25], there are four different injection locking cases defined by the frequency (or wavelength) relationship between the master laser and the free-running slave laser that result in different injection-locked cavity frequencies. The injection locking method used in our paper is just one of the four conditions mentioned. For simplicity, the master laser noises in our derivation are assumed to be 0. The following derivation has been modified to agree, after some simplifications, with the solution given in the tutorial. First of all, the injection-power-dependent threshold current of the VCSEL can be expressed as [4]

$$I_{\rm th,inj} = I_{\rm th} - \frac{qV\tau_p}{G_N\tau_s}\left[\frac{R_{\rm sp}}{S_{\rm Lm}} + \frac{2k_c\alpha}{\sqrt{1+\alpha^2}}\sqrt{\frac{S_{\rm inj}}{S_{\rm Lm}}}\right] \quad (1)$$

where $I_{\rm th}$ and $I_{\rm th,inj}$ denote the respective threshold currents of the VCSEL without and with external optical injection, q the electron charge, V the volume of the active region, τ_p and τ_s the photon lifetime and carrier lifetime, respectively, G_N the gain that varies linearly with the carrier density of newton per cubic centimeter, $R_{\rm sp}$ the spontaneous emission rate (expressed by $R_{\rm sp}/v_g = gn_{\rm sp}$ with $n_{\rm sp}$ referred to as the spontaneous emission factor), v_g the group velocity, $S_{\rm inj}$ the photon number injected into the laser cavity, $S_{\rm Lm}$ the maximum photon number in the injection-locked mode, α the linewidth enhancement factor,

and κ the coupling coefficient. The external injection essentially reduces the threshold of the VCSEL due to the increasing number of photons injected into the laser cavity. According to (1), the VCSEL threshold current will be reduced by 0.08 and 0.14 mA under the respective injection power of -10 and -5 dBm. The estimation is in rather good agreement with our experimental observations. According to the previously mentioned tutorial study [25], there are four different injection locking cases defined by the frequency (or wavelength) relationship between the master laser and the free-running slave laser that eventually result in different injection-locked cavity frequencies. In our case, the wavelength of the external injection is set to coincide with that of the free-running VCSEL so that a red-shifted wavelength (or decreased angular frequency) is observed for the VCSEL in the case of injection locking. The main effect of injection locking is an enlarged modulation bandwidth of the VCSEL since the external injection introduces additional carriers that change the carrier relaxation oscillation of the VCSEL. With the help of its power series expansion to the first-order term, the modified relaxation oscillation frequency (ω_R) of the VCSEL under external injection locking can be written as [12]

$$\begin{aligned}\omega_R &= \left[\frac{\Gamma v_g a}{qV}\eta_i\left(I - I_{\rm th} + \frac{qV\tau_p}{G_N\tau_s}\left[\frac{R_{\rm sp}}{S_{\rm Lm}} + \sqrt{\frac{4\alpha^2\kappa^2 S_{\rm inj}}{(1+\alpha^2)\,S_{\rm Lm}}}\right]\right)\right]^{1/2} \\ &\cong \left[\frac{\Gamma v_g a}{qV}\eta_i(I - I_{\rm th})\right]^{0.5}\left[1 + \frac{qV\tau_p}{2(I - I_{\rm th})G_N\tau_s} \times \left(\frac{R_{\rm sp}}{S_{\rm Lm}} + \frac{2\kappa\alpha}{\sqrt{1+\alpha^2}}\sqrt{\frac{S_{\rm inj}}{S_{\rm Lm}}}\right)\right] \\ &\cong \left[\frac{\Gamma v_g a}{qV}\eta_i(I - I_{\rm th})\right]^{0.5}\left[1 + \frac{qV\tau_p}{(I - I_{\rm th})G_N\tau_s} \times \left(\frac{\kappa\alpha}{\sqrt{1+\alpha^2}}\sqrt{\frac{S_{\rm inj}}{S_{\rm Lm}}}\right)\right] \qquad (2)\end{aligned}$$

where Γ denotes the confinement factor, a the differential gain, η_i the internal quantum efficiency, and I the biased current of the VCSEL. If $R_{\rm sp}$ is sufficiently small compared to the external injection, the result obtained is in fair agreement with the result given in the tutorial [25]. In particular, both include the factor $(\kappa\alpha/\sqrt{1+\alpha^2}) \times \sqrt{S_i/S_{\rm Lm}}$. It is clearly indicated in (2) that either an increase in the biased current or a boost in injection power can lead to an increase in the relaxation oscillation frequency of the VCSEL. According to (2), this is raised significantly under an external injection of -5 dBm, from 3 to 8.1 GHz, by increasing its dc bias from 1.2 to 1.4 mA. This is consistent with the experimental results, as shown in Fig. 2. Concurrently, the equivalent modulation bandwidth of the VCSEL can be enlarged to facilitate NRZ-to-RZ data format conversion at higher bit rates. To corroborate the improvement achieved by electrical pulse modulation, we demonstrate the enhancement of the directly modulated spectral response obtained by simultaneous electrical pulse modulation and optical injection.

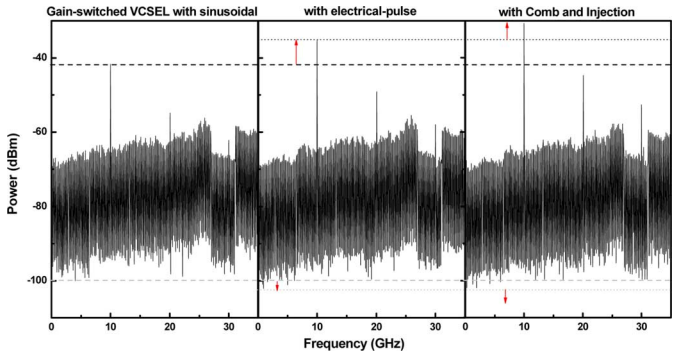

Fig. 5. Microwave spectra of NRZ-to-RZ convertor obtained with RBW at 100 kHz.

TABLE I
PEAK POWER OF THE MICROWAVE SIGNAL CONVERTED FROM THE OUTPUT OF THE VCSEL WITH DIFFERENT MODULATION FORMATS

	Peak Power (dBm)		
Frequency (GHz)	10	20	30
VCSEL w/sinusoidal	-41.7	-54.86	-62.2
VCSEL w/pulsed-signal	-35.1	-49.13	-57.96
VCSEL w/pulsed-signal and injection	-30.6	-44.3	-52.6

As shown by the microwave spectrum (see Fig. 5), the fundamental and harmonic frequency components of the VCSEL directly modulated at 10 GHz are greatly enhanced by using electrical pulse modulation accompanied by external injection.

Table I lists the measured output power at different harmonic frequencies for the VCSEL with different modulation formats. Both the RF power of the sinusoidal signal and the electrical pulse are 10.4 dBm. With only the sinusoidal wave modulation, the peak powers of the converted microwave signal at 10, 20, and 30 GHz are -41.7, -35.13, and -33.8 dBm, respectively. With only electrical pulse modulation, the microwave power of the frequency components at 10, 20, and 30 GHz is increased by 6.6, 5.7, and 4.3 dB, respectively. By simultaneously injecting the electrical-pulse modulated VCSEL with an optical source, the converted peak power obtained at 10, 20, and 30 GHz is further increased by 4.5, 4.8, and 5.3 dB compared to that obtained using electrical pulse modulation only (see black dashed and dotted lines in Fig. 5).

In comparison with a pure sinusoidal wave modulation, there is already a 6 dB increment in the power of the fundamental frequency component at 10 GHz. By external injection, both the fundamental and the harmonic frequency components of the electrical-pulse modulated VCSEL can be further enhanced by at least 4.5 dB. Apparently, the higher powers of the modulated frequency components are coupled to the VCSEL under electrical pulse modulation and external injection, thus leading to an improved direct modulation bandwidth of the VCSEL at 10 GHz. In particular, it was shown by the spectra that the direct electrical pulse modulation can also improve the SNR by greatly attenuating the noise level of the converted microwave spectrum (see the gray dashed and dotted lines in Fig. 5). By directly modulating the VCSEL with an electrical pulse, the low-frequency noise level of the converted microwave spectrum can be further

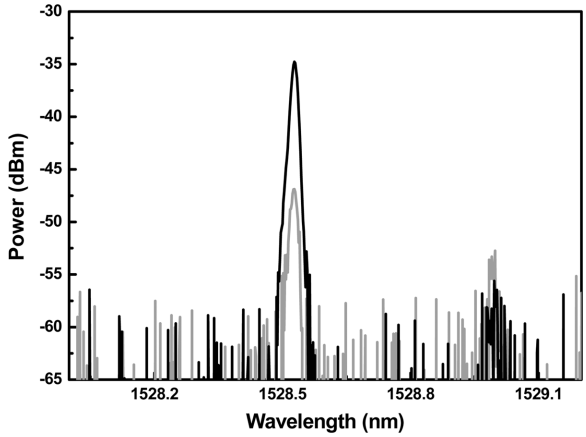

Fig. 6. Optical spectra of the VCSEL output with (black) and without (gray) injection.

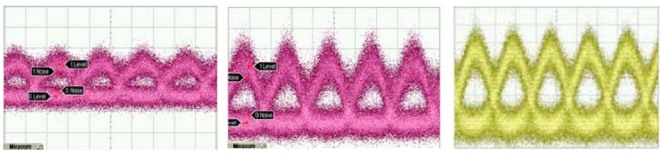

Fig. 7. Eye diagrams of the 10 Gbit/s RZ data at biased current of 1.2 mA (left), 1.3 mA (middle), and 1.4 mA (right).

decreased without and with external injection by 1 and 3 dB, respectively, compared to that employing a purely sinusoidal wave modulation. The estimated SNR of the VCSEL is raised from 3 to 5.4 dB by increasing the dc bias from 1.2 to 1.4 mA.

As evidence, the optical spectra of the VCSEL based RZ data generator with and without optical injection are shown in Fig. 6, where the side mode of the VCSEL under injection is suppressed by 40 dB compared to the main injection-locked mode. Raising the biased current of the VCSEL to achieve a larger modulation depth could effectively sharpen the RZ data shape and shorten the rising time of the RZ data, which improves the ER (defined as the log ratio of optical power at logic one (power of the pulse peak) to the optical power at logic zero (power of the dc level)) of the converted RZ data. The improved eye diagram of the EDFA-amplified RZ data stream generated from the VCSEL, by raising its biased current from 1.2 (10% below threshold current) to 1.4 mA, is shown in Fig. 7. The noisy eye diagram originates from the insufficient modulation bandwidth and the SNR of the VCSEL operated at slightly beyond threshold condition. The improvement on the measured ER in Fig. 7 with increasing dc bias of the VCSEL from 1.2 to 1.4 mA is mainly due to the sufficient carrier concentration in the VCSEL. This raises the relaxation oscillation of the VCSEL to a higher frequency. In contrast to the typical operation of the VCSEL directly modulated above threshold conditions, such an optical-injection-induced gain-switching VCSEL biased below or near threshold inevitably degrades its SNR and jitter performances due to the presence of a spontaneous emission component.

If the dc-biased current increases above threshold, both the single-sided band (SSB) phase noise and the ER are improved to provide a greatly reduced timing jitter of 3.7 ps. The gain

TABLE II
PARAMETRIC ANALYSIS OF THE CONVERTED RZ EYE DIAGRAM OUTPUT FROM THE VCSEL UNDER DIFFERENT BIASED CONDITIONS

Biased current (mA)		1.2	1.3	1.4
Injection ratio (dB)		26.6	16.8	12
$P_{receiving}$ (dBm)	BER @ 10^{-6}	-6	-20	-22
	BER @ 10^{-9}	--	-15	-19.5
ER (dB)		2.5	6.5	8.5
SNR (dB)		3	4.5	5.4
Jitter (ps)		17	3.7	2.9
Rising Time (ps)		24.1	13.0	8.3
Falling Time (ps)		25.6	13.2	9.1
Pulsewidth (ps)		56	29	23

switching mode is concurrently initiated to reshape the VCSEL output into a pulse-like RZ data stream with its pulsewidth shortened from 56 to 29 ps. However, since the transmission rate of a laser diode with the TO-can module is limited by the bonding wires, the directly modulated VCSEL is relatively difficult to be used at transmission rates up to 10 Gbit/s without specific design or operation. Although the gain-switched VCSEL can exceed the intrinsic bandwidth for 10 Gbit/s NRZ-to-RZ data format conversion by simultaneously using electrical pulse modulation and external injection, a finite dc bias prevents the breakdown of the homemade VCSEL from large electrical pulse modulation. Therefore, the degradation in the output RZ eye diagram occurs by operating a relatively low-biased VCSEL at extremely high bit rates.

For comparison, Table II lists all parameters concerning the performance of the converted RZ data pulses generated by the VCSEL at two biased conditions, where the optical injection ratio is defined as the ratio of the injection power to the output power of a freely running VCSEL. Although there is a larger amplitude fluctuation of the VCSEL output at a higher biased current, in this case, the RZ pulse still exhibits larger ER and lower timing jitter. With the given SNR and ER at different VCSEL dc biases in Table II, the Q-factor can be evaluated to greatly increase from 3.4 to 8.3, as calculated by $\mathrm{Q} \approx [(\mathrm{ER}-1)/(\mathrm{ER}+1)](\mathrm{M}\times\mathrm{SNR})^{0.5}$ at a receiver gain of 15 dB. Nonetheless, one should not be too optimistic about obtaining a better ER by simply operating the VCSEL biased current beyond the threshold condition since this could inevitably result in an RZ data stream with a larger dc offset causing ER degradation. On the other hand, increasing the biased current beyond the threshold condition is indeed a practical way to enhance the SNR, thus enhancing the BER performance by improving the Q-factor of the transmitted RZ data stream. However, the ER of the RZ output is decreased when the VCSEL bias is increased, which degrades the Q-factor as well as the transmission BER response. In this case, the optimization of the BER performance of the VCSEL generated RZ data stream requires a compromise between the dc-biased current and the electrical pulse modulation current.

Nevertheless, it is easily observed that the VCSEL exhibits a saturation behavior at a biased current larger than 5 mA, which indicates that the flattened top of the generated RZ pulse shape

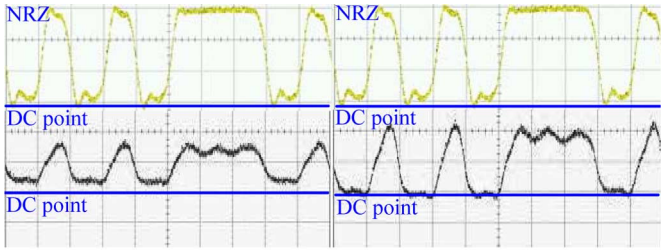

Fig. 8. Incoming "10101110" NRZ (upper) and the converted RZ (lower) data streams from the gain-switched VCSEL at injection power of -10 dBm and biased current of (a) 1.2 and (b) 1.3 mA.

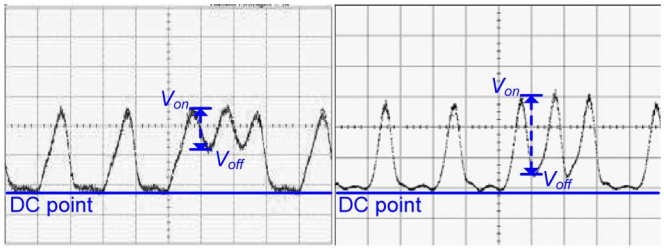

Fig. 9. (a) "10101110" RZ data streams from gain-switched VCSEL at biased current of (a) 1.3 and (b) 1.4 mA under injection power of -5 dBm.

could occur when driving the VCSEL up into the nonlinear modulation region. This is an inherent drawback of the homemade VCSEL, as compared to the commercially available one. Together with the aforementioned damage current, this sets an upper limit to the maximum peak modulation current for the homemade VCSEL. If the higher dc bias (>1.4 mA) of the VCSEL is employed while keeping the RF power at 10.4 dBm or larger, not only could the larger dc offset cause ER degradation of the converted RZ data, but also damage to the VCSEL could suddenly occur during operation. At the present stage, the VCSEL bias and the RF power of 1.4 mA and 10.4 dBm, respectively, are the most appropriate operation conditions for the homemade VCSEL used in our experiment. Figs. 8 and 9 illustrate four specific 10 Gbit/s RZ data streams obtained from the injection-locked VCSEL biased at 1.2, 1.3, and 1.4 mA under NRZ injection levels of -10 and -5 dBm. The monitored shapes of the converted RZ data streams indicate that the intrinsic bandwidth limitation of the VCSEL for an all-optical NRZ-to-RZ conversion is nearly 10 Gbit/s.

Although 10 GHz electrical pulse modulation is employed, the VCSEL biased at a smaller current still fails to gain-switch to generate shorter RZ data pulses due to the relatively long carrier recovery time of the VCSEL, as shown in Fig. 8(a). The VCSEL fails to respond to the consecutively incoming "ON" bits due to an intrinsic limitation on gain recovery and modulation bandwidth characteristics. A similar problem in reshaping the RZ pulse is encountered when attenuating the optical NRZ injection power from -5 to -10 dBm, as shown in Fig. 8(b). In comparison with the data stream shown in Fig. 9(a), the generated RZ data streams in Fig. 9(b) show a sharper shape between adjacent bits because the VCSEL is biased at a higher dc current. With consecutively incoming "ON" bits at an injection power of -5 dBm, the ER is increased greatly, from 3 to 8.5 dB, by enlarging the VCSEL biased current from 1.3 to 1.4 mA. In Fig. 9, the ER between adjacent data bits is enhanced by combining it with the injection-induced threshold current reduction effect, thus providing at least 5.5 dB improvement by equivalently up offsetting the dc bias level of the VCSEL from $I_{\rm th}+0.14$ mA to $I_{\rm th}+0.24$ mA. We attribute that this is to the enhanced stimulated emission as compared to the spontaneous one. However, the ER of the VCSEL-converted RZ data stream degrades again when the VCSEL bias is further increased to 1.5 mA or more, and the transmission performance slightly degrades accordingly. Another important parameter affecting the NRZ-to-RZ data conversion and the transmission performance of the VCSEL is the dynamic chirp associated with the converted RZ data.

We have derived the rate equation for the transient VCSEL output phase in order to examine the influence of the external injection power and a biased current, and we have characterized the linewidth and chirp of the pulsed RZ data generated from the injection-locked VCSEL under gain-switched conditions. In the Appendix , the dynamic chirp of the RZ data generated from the externally NRZ injection-locked VCSEL can be derived as

$$\Delta v(t) = -\frac{1}{2\pi}\left\{\frac{\alpha g}{2}\left[N(t) - \left(N_{\rm th} - \frac{2\kappa}{g\sqrt{1+\alpha^2}}\sqrt{\frac{S_{\rm inj}}{S_{\rm Lm}}}\right)\right]\right\}. \tag{3}$$

In (3), the peak-to-peak variation of the chirped frequency is enlarged by increasing either the injection power or the biased current (see Figs. 10 and 11). In the meantime, the linewidth of the VCSEL output [26] should also be modified as (4), shown at the bottom of the page, where $\alpha = -(\delta n'/\delta N)/(\delta n''/\delta N) = -4\pi(dn/dg)/\lambda$ is the linewidth enhancement factor with n' and n'' denoting the real and imaginary parts of the refractive index and dn and dg denoting the small index and optical gain variations under the variation δN of the carrier density by external injection. Equations (3) and (4) reveal that the enlarged chirp and the broadened linewidth are straightforward consequences of the RZ data stream generated from the gain-switched VCSEL under externally NRZ injection-locked conditions.

These effects show that the fine tuning of the operating parameters of the VCSEL based NRZ-to-RZ converter is

$$\Delta f = \frac{K_{\rm total}R_{\rm sp}(\alpha^2+1)}{\left[4\pi\eta_i/(v_g(\alpha_m+\alpha_i)\tau_c)\right]\cdot\left[N - N_{\rm th} + (2\kappa/g)(1/\sqrt{1+\alpha^2})(\sqrt{S_{\rm inj}/S_{\rm Lm}})\right]} \tag{4}$$

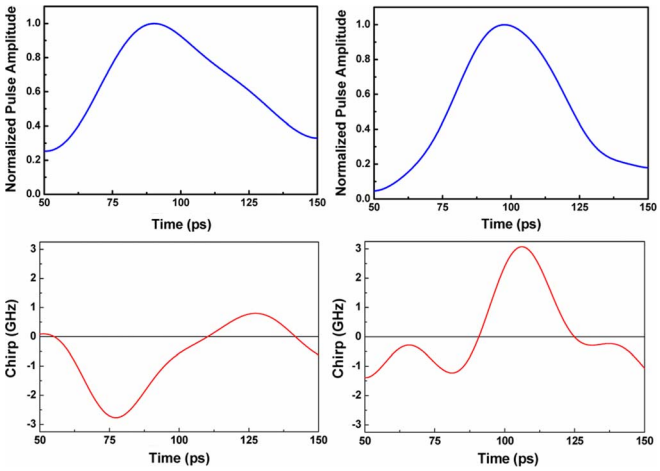

Fig. 10. Traces (up) and chirp (down) of the generated RZ data streams from VCSEL biased at 1.2 mA under external NRZ injection power of -10 dBm (left) and -5 dBm (right).

of particular importance for minimizing the degradation of the transmission performance at higher bit rates. The corresponding peak-to-peak chirps of the converted RZ data streams with changing NRZ injection powers are shown in Fig. 10. The dc level of the RZ data stream is slightly decreased by raising the optical NRZ injection power since the external injection can attenuate the continuous wave lasing component intensity in the VCSEL cavity. This is due to the cross-gain modulation-induced suppression mechanism. It is also found that the positive frequency chirp is larger than the negative one due to the lengthened falling time of the VCSEL switching response. The peak-to-peak chirps of the RZ data streams generated from the 1.2-mA biased VCSEL under NRZ injection powers of -10 and -5 dBm are 3.6 and 4.3 GHz, respectively. The corresponding chirp parameter of the converted RZ data is increased from 60 to 122 MHz/ps if the NRZ injection power is raised by 5 dB. The variation in carrier concentration is coupled with a change in the refractive index, the effective cavity length, and the resonant frequency. With higher injecting power, to effectively reduce the threshold current, the larger positive chirp at the rising edge can be seen in the lower right part of Fig. 10. This correlates well with the increasing carrier accumulation in the VCSEL. In addition, the peak-to-peak chirp is significantly delayed due to a longer accumulation time required for carriers to recover in the VCSEL cavity. In comparison, Fig. 11 illustrates the optical pulses (dash line) and corresponding peak-to-peak chirps (solid line) of the RZ data from the VCSEL by changing dc-biased current under an NRZ injection power of -5 dBm. As shown in (4) , the linewidth of the RZ data pulse is proportional to the linewidth enhancement factor and the reciprocal output power so that the phase variation of the RZ data pulse is strongly correlated with the power change in the VCSEL cavity. The output power is also increased and the carrier accumulation enhanced when the VCSEL biased current is raised, whereas the linewidth enhancement factor is decreased due to the increased gain variation in the VCSEL. In this case, the RZ data pulsewidth becomes shorter even though the $n_{\rm sp}$ is increased.

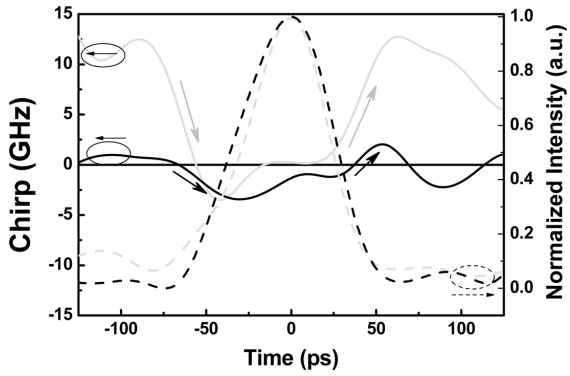

Fig. 11. Pulse shapes and chirps of the RZ data bit at biased current of 1.2 (blue line) and 1.3 mA (red line) under NRZ injection power of -5 dBm.

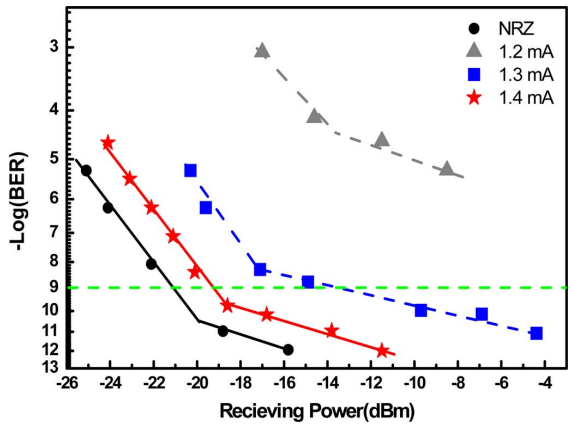

Fig. 12. BER analysis of the optical NRZ from a externally modulated VCSEL without injection (black), and the generated RZ at 10 Gbit/s from the injection-locked VCSEL at biased current of 1.2 mA (gray), 1.3 mA (blue), and 1.4 mA (red).

The coherence between mode frequency and injection frequency in the VCSEL is improved so that the relaxation–oscillation frequency greatly increases and the RZ data pulsewidth decreases under higher optical power injection. Finally, the BER performance of the back-to-back transmission of the RZ data at 10 Gbit/s is shown in Fig. 12. This indicates that an optical receiving power of at least -19.5 dBm is required to obtain a BER of 10^{-9} at a biased current of 1.4 mA with -5 dBm optical NRZ injection. This is 4.5 dB better than the one obtained by a lower biased current of 1.3 mA. Such a receiving sensitivity is still 1.5 dB lower than that of the NRZ data transmission obtained by externally NRZ-modulating the VCSEL. Nonetheless, these results have demonstrated the possibility of operating the VCSEL based NRZ-to-RZ data stream converter beyond its original modulation bandwidth. The RZ data generation completely diminishes by detuning the VCSEL bias below 90% of its threshold current, while the receiving power required for $\mathrm{BER} = 10^{-6}$ inevitably increases to -6 dBm. In contrast, the BER can be improved by five orders of magnitude by increasing the VCSEL bias from 1.2 to 1.3 mA (approaching the lasing threshold), corresponding to a negative power penalty of -12 dB at the same BER level.

In particular, the slope of the BER versus receiving power significantly changes at a receiving power of >-19 dBm. This

illustrates a finite improvement on the ER between adjacent RZ data bits that can be obtained by increasing the receiving power. At a receiving power below -18.5 dBm, the greatly decreased ER and the significantly enlarged timing jitter inevitably cause serious degradation of the BER performance. This is mainly due to the amplified spontaneous emission (ASE) induced deterministic-jitter in the VCSEL and to the cross-point change with lengthened rising and falling times. In addition, increasing the NRZ injection power causes more carriers to remain within the VCSEL cavity for a longer carrier accumulation time so that the peak of the RZ data pulse is slightly delayed due to the so-called pattern effect that is often caused by the slow carrier recovery in semiconductor laser diodes. The major reason for the slope change in the BER curves is crosstalk between the reflected incoming optical NRZ injection and the output of the VCSEL converted RZ data stream. With a limited receiving sensitivity of the 10 Gbit/s lightwave receiver (Agilent 83434A), the VCSEL converted RZ data stream inevitably introduces a noise floor in its BER response. Increasing the dc bias helps to reduce the receiving power penalty and the occurrence power of the BER noise floor. However, the ultimate limitation is determined by the end-face reflection of such an injection locking system rather than by other parameters.

IV. Conclusion

A TO-46-can packaged VCSEL with a finite bandwidth of only 3 GHz has been employed to demonstrate a 10-Gbit/s all-optical NRZ-to-RZ data format convertor. This approach is based on the injection-locking induced gain switching and the beyond-bandwidth electrical pulse modulation of the TO-46-can packaged VCSEL biased at nearly lasing condition. To support 10 Gbit/s RZ data pulse generation, the resonant relaxation oscillation frequency of this TO-46-can packaged VCSEL is increased through direct modulation by an electrical pulse at 10 GHz and external NRZ optical injection from 2 to at least 7.3 GHz. The optimized 10 Gbit/s RZ data stream exhibits the SNR, the timing jitter, and the pulsewidth of 7.2 dB, 2.9 ps, and 27 ps, respectively. The peak-to-peak chirp and corresponding chirp parameter are slightly raised to 4.3 GHz and 122 MHz/ps by increasing the injection power and the biased current. Owing to carrier accumulation and gain variation, the RZ data pulsewidth gets reduced by increasing the optical NRZ injection power and concurrently increasing the dc-biased current. A higher dc-biased current further promotes the RZ data with greater modulation depth and sharper shape. A BER of 10^{-9} at 10 Gbit/s is achieved at a receiving power of -19.5 dBm, and an improvement of receiving power penalties up to 16 dB is observed when the dc-biased current is reduced to only 10% of its lasing threshold. Despite the finite bandwidth set by the homemade VCSEL, this paper demonstrates the feasibility of operating the TO-can packaged VCSEL based RZ generator beyond its intrinsic modulation bandwidth with the aid of electrical pulse modulation and externally optical injection. Most concerns regarding the noisy data stream output can be addressed if the VCSEL can tolerate a larger bias and thereby achieve a better SNR before breakdown.

Appendix
Derivation of the Rate Equations for Output Power, Frequency Chirp, and Linewidth

The rate equations of the injection-locked VCSEL under external injection used in our paper are listed as bellow (by simply quoting the equation employed in [25])

$$\frac{dS(t)}{dt} = \frac{1}{2}[g(N(t)-N_{\rm tr})-\gamma_p]S(t) + \kappa\sqrt{S_{\rm inj}}\cos(\phi(t)) \tag{A1}$$

$$\frac{d\phi(t)}{dt} = \frac{\alpha}{2}[g(N(t)-N_{\rm tr})-\gamma_p] - \kappa\sqrt{\frac{S_{\rm inj}}{S_{\rm Lm}}}\sin\,\phi(t) - \Delta w_{\rm inj} \tag{A2}$$

where $S(t)$ denotes the slave laser's photo number, g the stimulated emission rate, N the carrier number, $N_{\rm tr}$ the slave laser's transparency carrier number, γ_p the photo decay rate, κ the coupling rate, $S_{\rm inj}$ the injected photo number, α the linewidth enhancement factor, $S_{\rm Lm}$ the maximum photo number in the injection-locked mode, $\Delta w_{\rm inj}$ the detuning frequency, and $\phi(t)$ denotes the phase difference between the internal and injected fields, as expressed by $\phi(t) = \psi(t) - \Delta w_{\rm inj}t - \psi_{\rm inj}$, where $\psi(t)$ and $\psi_{\rm inj}$ are the phase of the injection-locked VCSEL and the constant phase of the injection-locked VCSEL output under external injection. The aforementioned phase rate equation can be simplified after solving the steady-state solution of the injection-locked VCSEL. By simply taking the solutions given by Murakami *et al.* [27], the phase difference $\phi(t)$ under steady-state condition can be described as

$$\phi_s = \sin^{-1}\left\{-\frac{\Delta w_{\rm inj}}{k\sqrt{1+\alpha^2}}\sqrt{\frac{S_{\rm Lm}}{S_{\rm ing}}}\right\} - \tan^{-1}\alpha = -\tan^{-1}\alpha. \tag{A3}$$

With a small-signal approximation of $d\phi(t)/dt = 2\pi\Delta v(t)$ under a specific injection locking condition of $\Delta w_{\rm inj} = 0$, the dynamic chirp can further be simplified as

$$\begin{aligned}
\Delta v(t) &= -\frac{1}{2\pi}\frac{d\phi(t)}{dt} \\
&= -\frac{1}{2\pi}\left\{\begin{array}{l}\frac{\alpha}{2}\left[g[N(t)-N_{\rm tr}]-\gamma_p\right] \\ -\kappa\sqrt{\frac{S_{\rm inj}}{S_{\rm Lm}}}\sin\left(\phi(t)-\phi_{\rm inj}\right)-\Delta w_{\rm inj}\end{array}\right\} \\
&= -\frac{1}{2\pi}\left\{\begin{array}{l}\frac{\alpha}{2}g[N(t)-N_{\rm th}] \\ -k\sqrt{\frac{S_{\rm inj}}{S_{\rm Lm}}}\sin\left(\phi(t)-\phi_{\rm inj}\right)-\Delta w_{\rm inj}\end{array}\right\} \\
&\qquad\qquad \left(\text{with } N_{\rm th} \equiv N_{\rm tr} + \tfrac{\gamma_p}{g}\right) \\
&= -\frac{1}{2\pi}\left\{\begin{array}{l}\frac{\alpha}{2}g[N(t)-N_{\rm th}] \\ -\kappa\sqrt{\frac{S_{\rm inj}}{S_{\rm Lm}}}\sin\left(\phi(t)-\phi_{\rm inj}\right)-\Delta w_{\rm inj}\end{array}\right\} \\
&\qquad\qquad (\text{with } \Delta w_{\rm inj} \equiv 0) \\
&= -\frac{1}{2\pi}\left\{\frac{\alpha}{2}g[N(t)-N_{\rm th}] - \kappa\sqrt{\frac{S_{\rm inj}}{S_{\rm Lm}}}\sin\left(\phi_s\right)\right\}.
\end{aligned} \tag{A4}$$

Under steady-state condition, we have (A5), shown at the bottom of the page, with specific injection locking condition, $\Delta w_{\rm inj}$ approaches 0. Therefore, the frequency chirp can be obtained as

$$\begin{aligned}
&\Delta v(t)\\
&\quad=-\frac{1}{2\pi}\left\{\frac{\alpha}{2}g[N(t)-N_{\rm th}]+\frac{\kappa\alpha}{\sqrt{1+\alpha^2}}\sqrt{\frac{S_{\rm inj}}{S_{\rm Lm}}}\right\}\\
&\quad=-\frac{1}{2\pi}\left\{\frac{\alpha}{2}g\left[N(t)-N_{\rm th}+\frac{2\kappa}{g\sqrt{1+\alpha^2}}\sqrt{\frac{S_{\rm inj}}{S_{\rm Lm}}}\right]\right\}\\
&\quad=-\frac{1}{2\pi}\left\{\frac{\alpha}{2}g\left[N(t)-\left(N_{\rm th}-\frac{2\kappa}{g\sqrt{1+\alpha^2}}\sqrt{\frac{S_{\rm inj}}{S_{\rm Lm}}}\right)\right]\right\}\\
&\quad=-\frac{\alpha}{4\pi}g[N(t)-N'_{\rm th}]\\
&\quad=\Delta v_0(t)+\Delta v_{\rm inj}(t).
\end{aligned}\tag{A6}$$

Besides, by taking the steady-state value ϕ_s, the aforementioned threshold carrier number of the injection-locked VCSEL can be described (assuming that $\Delta w_{\rm inj}=0$ in our case), shown in (A7) at the bottom of the page.

Thus, the injection-locked VCSEL output power can be rewritten as [28]

$$\begin{aligned}
P_{\rm out}&=\frac{\eta_h h\nu}{q}\frac{\alpha_{\rm mir}}{(\alpha_{\rm mir}+\alpha_{\rm int})}(I-I_{\rm th}+I_{\rm inj})\\
&=\frac{\eta_h h\nu}{q}\frac{\alpha_{\rm mir}}{(\alpha_{\rm mir}+\alpha_{\rm int})}\left[\frac{q}{\tau_s}(N-N_{\rm th}-\Delta N_s)\right]\\
&=\frac{\eta_h h\nu}{\tau_s}\frac{\alpha_{\rm mir}}{(\alpha_{\rm mir}+\alpha_{\rm int})}(N-N_{\rm th}-\Delta N_s)\\
&=\frac{\eta_h h\nu}{\tau_s}\frac{\alpha_{\rm mir}}{(\alpha_{\rm mir}+\alpha_{\rm int})}\\
&\quad\times\left(N-N_{\rm th}+\frac{2\kappa}{g}\frac{1}{\sqrt{1+\alpha^2}}\sqrt{\frac{S_{\rm inj}}{S_{\rm Lm}}}\right)\\
&=\frac{\eta_h h\nu}{\tau_s}\frac{\alpha_{\rm mir}}{(\alpha_{\rm mir}+\alpha_{\rm int})}\\
&\quad\times\left(N-N_{\rm th}+\frac{2\kappa}{g}\frac{1}{\sqrt{1+\alpha^2}}\sqrt{\frac{S_{\rm inj}}{S_{\rm Lm}}}\right)\\
&=\frac{\eta_h h\nu\alpha_{\rm eff}}{\tau_s}\left(N-N_{\rm th}+\frac{2\kappa}{g}\frac{1}{\sqrt{1+\alpha^2}}\sqrt{\frac{S_{\rm inj}}{S_{\rm Lm}}}\right)\\
&=\frac{\eta_{\rm int} h\nu\alpha_{\rm eff}}{\tau_s}[N-N'_{\rm th}]
\end{aligned}\tag{A8}$$

$$\begin{aligned}
\Delta v(t)&=-\frac{1}{2\pi}\left\{\begin{array}{l}\frac{\alpha}{2}g[N(t)-N_{\rm th}]\\ -\kappa\sqrt{\frac{S_{\rm inj}}{S_{\rm Lm}}}\sin\left(\sin^{-1}\left(-\frac{\Delta w_{\rm inj}}{k\sqrt{1+\alpha^2}}\sqrt{\frac{S_{\rm Lm}}{S_{\rm inj}}}\right)-\tan^{-1}\alpha\right)\end{array}\right\}\\
&=-\frac{1}{2\pi}\left\{\begin{array}{l}\frac{\alpha}{2}g[N(t)-N_{\rm th}]\\ -\kappa\sqrt{\frac{S_{\rm inj}}{S_{\rm Lm}}}\left[\begin{array}{l}\left(-\frac{\Delta w_{\rm inj}}{k\sqrt{1+\alpha^2}}\sqrt{\frac{S_{\rm Lm}}{S_{\rm inj}}}\right)\cos\left(\tan^{-1}\alpha\right)\\ -\sin\left(\tan^{-1}\alpha\right)\cos\left(\sin^{-1}\left(-\frac{\Delta w_{\rm inj}}{k\sqrt{1+\alpha^2}}\sqrt{\frac{S_{\rm Lm}}{S_{\rm inj}}}\right)\right)\end{array}\right]\end{array}\right\}\\
&=-\frac{1}{2\pi}\left\{\begin{array}{l}\frac{\alpha}{2}g[N(t)-N_{\rm th}]\\ -\kappa\sqrt{\frac{S_{\rm inj}}{S_{\rm Lm}}}\left[\begin{array}{l}\left(-\frac{\Delta w_{\rm inj}}{k\sqrt{1+\alpha^2}}\sqrt{\frac{S_{\rm Lm}}{S_{\rm inj}}}\right)\frac{1}{\sqrt{1+\alpha^2}}\\ -\frac{\alpha}{\sqrt{1+\alpha^2}}\sqrt{1-\frac{\Delta w_{\rm inj}^2 S_{\rm Lm}}{\kappa^2(1+\alpha^2)S_{\rm inj}}}\end{array}\right]\end{array}\right\}
\end{aligned}\tag{A5}$$

$$\begin{aligned}
\Delta N_s&=-\frac{2\kappa}{g}\sqrt{\frac{S_{\rm inj}}{S_{\rm Lm}}}\cos\ \phi_s\\
&=-\frac{2\kappa}{g}\sqrt{\frac{S_{\rm inj}}{S_{\rm Lm}}}\cos\left[\sin^{-1}\left(-\frac{\Delta w_{\rm inj}}{k\sqrt{1+\alpha^2}}\sqrt{\frac{S_{\rm Lm}}{S_{\rm inj}}}\right)-\tan^{-1}\alpha\right]\\
&=-\frac{2\kappa}{g}\sqrt{\frac{S_{\rm inj}}{S_{\rm Lm}}}\left\{\begin{array}{l}\cos\left[\sin^{-1}\left(-\frac{\Delta w_{\rm inj}}{k\sqrt{1+\alpha^2}}\sqrt{\frac{S_{\rm Lm}}{S_{\rm inj}}}\right)\right]\cos\left(\tan^{-1}\alpha\right)\\ +\sin\left[\sin^{-1}\left(-\frac{\Delta w_{\rm inj}}{k\sqrt{1+\alpha^2}}\sqrt{\frac{S_{\rm Lm}}{S_{\rm inj}}}\right)\right]\sin\left(\tan^{-1}\alpha\right)\end{array}\right\}\\
&=-\frac{2\kappa}{g}\sqrt{\frac{S_{\rm inj}}{S_{\rm Lm}}}\left\{\begin{array}{l}\sqrt{1-\frac{\Delta w_{\rm inj}^2 S_{\rm Lm}}{\kappa^2(1+\alpha^2)S_{\rm inj}}}\frac{1}{\sqrt{1+\alpha^2}}\\ +\left(-\frac{\Delta w_{\rm inj}}{k\sqrt{1+\alpha^2}}\sqrt{\frac{S_{\rm Lm}}{S_{\rm inj}}}\right)\frac{\alpha}{\sqrt{1+\alpha^2}}\end{array}\right\}\\
&=-\frac{2\kappa}{g}\frac{1}{\sqrt{1+\alpha^2}}\sqrt{\frac{S_{\rm inj}}{S_{\rm Lm}}}
\end{aligned}\tag{A7}$$

where hv denotes the energy per photon, q the electron charge, v_g the group velocity, α_m the facet loss, η_i the internal quantum efficiency, I the biased current of the VCSEL, $\langle\alpha_i\rangle$ the internal loss of the VCSEL, τ_p and τ_s the photon lifetime and carrier lifetime, and $\alpha_{\text{eff}} = [\alpha_m/(\langle\alpha_i\rangle + \alpha_m)]$ denotes the effective loss factor contributed by the resonant cavity reflector of the VCSEL, shown in (A9) at the bottom of the page.

The mean frequency deviation of the VCSEL under external injection locking condition (with respect to the reference angular frequency w_{th}) can be described as [26]

$$\langle\dot{\phi}\rangle = \left\langle\frac{d\phi}{dt}\right\rangle = \frac{\alpha}{2}g\langle N' - N_{\text{th}}\rangle \tag{A10}$$

where the $N' = N + N_{\text{inj}}$ and the frequency difference is given by

$$\delta\dot{\phi} = \dot{\phi} - \langle\dot{\phi}\rangle = \frac{\alpha}{2}g\langle N' - \langle N'\rangle\rangle + F_\phi(t) \tag{A11}$$

where $F_\phi(t)$ denotes the spontaneous noise. After Fourier transformation

$$\delta\dot{\phi}(w_m) = \frac{1}{2}g\Delta n(w_m) + \Delta F_\phi(w_m) \tag{A12}$$

where $\Delta n(wm)$ denotes the carrier noise that is obtained as

$$\Delta n(w_m) = -H(jw)\frac{\Delta F_s(w_m)}{w_r^2\tau_{\text{ph}}V}. \tag{A13}$$

By replacing $w_r^2 = \langle S'\rangle g/\tau_{\text{ph}}V$ into the aforementioned equation, we have

$$\Delta\dot{\phi}(w_m) = -\frac{\alpha}{2\langle S'\rangle}H(jw_m)\Delta F_s(w_m) + \Delta F_\phi(w_m). \tag{A14}$$

Thus, the spectral density can be described as

$$\begin{aligned} W_{\dot{\phi}} &= \langle|\Delta\dot{\phi}(w_m)|^2\rangle \\ &= |H(jw_m)|^2\langle|\Delta F_s(w_m)|^2\rangle\left(\frac{\alpha}{2\langle S'\rangle}\right)^2 \\ &\quad + \langle|\Delta F_\phi(w_m)|^2\rangle \end{aligned} \tag{A15}$$

where $\langle|\Delta F_s(w_m)|^2\rangle = 2\langle S'\rangle K_{\text{total}}R_{\text{sp}}$ and $\langle|\Delta F_\phi(w_m)|^2\rangle = K_{\text{total}}R_{\text{sp}}/2\langle S'\rangle$.

In this case

$$W_{\dot{\phi}} = \frac{K_{\text{total}}R_{\text{sp}}}{2\langle S'\rangle}(\alpha^2|H(jw_m)| + 1) = \frac{K_{\text{total}}R_{\text{sp}}}{2\langle S'\rangle}(\alpha^2 + 1) \tag{A16}$$

$$\begin{aligned}
\Delta\phi(t) &= \left\{\frac{\alpha}{2}[g(N(t) - N_{\text{th}})] - \kappa\sqrt{\frac{S_{\text{inj}}}{S_{\text{Lm}}}}\sin\phi_s - \Delta w_{\text{inj}}\right\}t \\
&= \left\{\begin{array}{l} \frac{\alpha}{2}\left[g(N(t) - N_{\text{th}})\right] \\ -\kappa\sqrt{\frac{S_{\text{inj}}}{S_{\text{Lm}}}}\sin\left[\sin^{-1}\left(-\frac{\Delta w_{\text{inj}}}{\kappa\sqrt{1+\alpha^2}}\sqrt{\frac{S_{\text{Lm}}}{S_{\text{inj}}}}\right) - \tan^{-1}\ \alpha\right] \\ -\Delta w_{\text{inj}} \end{array}\right\}t \\
&= \left\{\begin{array}{l} \frac{\alpha}{2}\left[g(N(t) - N_{\text{th}})\right] \\ -\kappa\sqrt{\frac{S_{\text{inj}}}{S_{\text{Lm}}}}\left[-\frac{\Delta w_{\text{inj}}}{\kappa\sqrt{1+\alpha^2}}\sqrt{\frac{S_{\text{Lm}}}{S_{\text{inj}}}}\frac{1}{\sqrt{1+\alpha^2}}\right. \\ \left.-\sqrt{1-\left(\frac{\Delta w_{\text{inj}}}{\kappa\sqrt{1+\alpha^2}}\sqrt{\frac{S_{\text{Lm}}}{S_{\text{inj}}}}\right)^2}\frac{\alpha}{\sqrt{1+\alpha^2}}\right] - \Delta w_{\text{inj}} \end{array}\right\}t \\
&= \left\{\begin{array}{l} \frac{\alpha}{2}\left[g(N(t) - N_{\text{th}})\right] \\ +\frac{\Delta w_{\text{inj}}}{1+\alpha^2} + \sqrt{\left(\frac{\kappa^4\alpha^2(1+\alpha^2)S_{\text{inj}}^2 - \kappa^2\alpha^2\Delta w_{\text{inj}}^2 S_{\text{Lm}}S_{\text{inj}}}{\kappa^2(1+\alpha^2)^2 S_{\text{Lm}}S_{\text{inj}}}\right)} - \Delta w_{\text{inj}} \end{array}\right\}t \\
&\cong \left\{\frac{\alpha}{2}\left[g(N(t) - N_{\text{th}})\right] + \sqrt{\frac{\kappa^2\alpha^2 S_{\text{inj}}}{(1+\alpha^2)S_{\text{Lm}}}}\right\}t \\
&\qquad\qquad\qquad\qquad\qquad\qquad\qquad\qquad\qquad\qquad\qquad\qquad\qquad \text{(by setting } \Delta w_{\text{inj}} \equiv 0) \\
&= \left\{\frac{\alpha}{2}\left[g(N(t) - N_{\text{th}})\right] + \frac{\kappa\alpha}{\sqrt{1+\alpha^2}}\sqrt{\frac{S_{\text{inj}}}{S_{\text{Lm}}}}\right\}t \\
&= \left\{\frac{\alpha}{2}g\left[N(t) - N_{\text{th}} + \frac{2\kappa}{g\sqrt{1+\alpha^2}}\sqrt{\frac{S_{\text{inj}}}{S_{\text{Lm}}}}\right]\right\}t \\
&= \left\{\frac{\alpha}{2}g\left[N(t) - \left(N_{\text{th}} - \frac{2\kappa}{g\sqrt{1+\alpha^2}}\sqrt{\frac{S_{\text{inj}}}{S_{\text{Lm}}}}\right)\right]\right\}t \\
&= \left\{\frac{\alpha}{2}g\left[N(t) - N'_{\text{th}}\right]\right\}t = \{\Delta\phi_0 + \Delta\phi_{\text{inj}}\}t.
\end{aligned} \tag{A9}$$

$$\Delta f = \frac{W_{\dot{\phi}}}{2\pi} = \frac{K_{\text{total}}R_{\text{sp}}}{4\pi\langle S'\rangle}(\alpha^2+1) = \frac{K_{\text{total}}R_{\text{sp}}}{4\pi\left(P_{\text{out}}/h\nu v_g\alpha_m\right)}(\alpha^2+1)$$
$$= \frac{K_{\text{total}}R_{\text{sp}}(\alpha^2+1)}{(4\pi/h\nu v_g\alpha_m)\left((\eta_i h\nu\alpha_{\text{eff}}/\tau_c)\left[N-N_{\text{th}}+(2\kappa/g)(1/\sqrt{1+\alpha^2})(\sqrt{S_{\text{inj}}/S_{\text{Lm}}})\right]\right)}$$
$$= \frac{K_{\text{total}}R_{\text{sp}}(\alpha^2+1)}{(4\pi\eta_i/v_g(\alpha_m+\alpha_i)\tau_c)\left[N-N_{\text{th}}+(2\kappa/g)(1/\sqrt{1+\alpha^2})(\sqrt{S_{\text{inj}}/S_{\text{Lm}}})\right]}. \quad \text{(A17)}$$

Therefore, the linewidth of the injection-locked VCSEL output should be modified as shown in (A17) at the top of the page.

REFERENCES

[1] S. Bigo, E. Desurvire, S. Gauchard, and E. Brun, "Bit-rate enhancement through optical NRZ-to-RZ conversion and passive time-division multiplexing for soliton transmission systems," *Electron. Lett.*, vol. 30, no. 4, pp. 984–985, Jun. 1994.

[2] D. Norte and A. E. Willner, "Demonstration of an all-optical data format transparent WDM-to-TDM network node with extinction ratio enhancement for reconfigurable WDM networks," *IEEE Photon. Technol. Lett.*, vol. 8, no. 5, pp. 715–717, May 1996.

[3] C. W. Chow, C. S. Wong, and H. K. Tsang, "All-optical NRZ to RZ format and wavelength converter by dual-wavelength injection locking ," *Opt. Commun.*, vol. 209, pp. 329–334, Aug. 2002.

[4] Y. C. Chang, Y. H. Lin, J. H. Chen, and G. R. Lin, "All-optical NRZ-to-PRZ format transformer with an injection-locked Fabry–Perot laser diode at unlasing condition," *Opt. Exp.*, vol. 12, no. 19, pp. 4449–4456, Sep. 2004.

[5] L. Noel, X. Shan, and A. D. Ellis, "Four WDM channel NRZ to RZ format conversion using a single semiconductor laser amplifier ," *Electron. Lett.*, vol. 31, no. 4, pp. 277–278, Feb. 1995.

[6] H. J. Lee, H. G. Kim, J. Y. Choi, and H. K. Lee, "All-optical clock recovery from NRZ data with simple NRZ-to-PRZ converter based on self-phase modulation of semiconductor optical amplifier," *Electron. Lett.*, vol. 35, no. 12, pp. 989–990, Jun. 1999.

[7] Y. D. Jeong, H. J. Lee, H. Yoo, and Y. H. Won, "All-optical NRZ-to-PRZ converter at 10 Gb/s based on self-phase modulation of Fabry–Perot laser diode ," *IEEE Photon. Technol. Lett.*, vol. 16, no. 4, pp. 1179–1181, Apr. 2004.

[8] L. Huo, Y. Dong, C. Lou, and Y. Gao, "Clock extraction using an optoelectronic oscillator from high-speed NRZ signal and NRZ-to-RZ format transformation," *IEEE Photon. Technol. Lett.*, vol. 15, no. 7, pp. 981–983, Jul. 2003.

[9] J. Wang, J. Q. Sun, Q. Z. Sun, D. L. Wang, M. J. Zhou, X. L. Zhang, D. X. Huang, and M. M. Fejer, "Experimental observation of all-optical nonreturn-to-zero-to-return-to-zero format conversion based on cascaded second-order nonlinearity assisted by active mode-locking," *Opt. Lett.*, vol. 32, no. 16, pp. 2462–2464, Aug. 2007.

[10] A. Buxens, H. N. Poulsen, A. T. Clausen, and P. Jeppesen, "All-optical OTDM-to-WDM signal-format translation and OTDM add-drop functionality using bidirectional four wave mixing in semiconductor optical amplifier," *Electron. Lett.*, vol. 36, no. 2, pp. 156–158, Jan. 2000.

[11] L. P. Barry, P. Anandarajah, and A. Kaszubowsk, "Optical pulse generation at frequencies up to 20 GHz using external-injection seeding of a gain-switched commercial Fabry–Perot laser," *IEEE Photon. Technol. Lett.*, vol. 13, no. 9, pp. 1014–1016, Sep. 2001.

[12] W. Hofmann, M. Müller, A. Nadtochiy, C. Meltzer, A. Mutig, G. Böhm, J. Rosskopf, D. Bimberg, M.-C. Amann, and C. J. Chang-Hasnain, "22-Gb/s long wavelength VCSELs," *Opt. Exp.*, vol. 17, no. 20, pp. 17547–17554, Sep. 2009.

[13] W. Hofmann, L. Grüner-Nielsen, E. Rönneberg, G. Böhm, M. Ortsiefer, and M. C. Amann, "1.55-μm VCSEL modulation performance with dispersion-compensating fibers," *IEEE Photon. Technol. Lett.*, vol. 21, no. 15, pp. 1072–1074, Aug. 2009.

[14] D. Parekh, X. Zhao, W. Hofmann, M. C. Amann, L. A. Zenteno, and C. J. Chang-Hasnain, "Greatly enhanced modulation response of injection-locked multimode VCSELs," *Opt. Exp.*, vol. 16, no. 26, pp. 21582–21586, Dec. 2008.

[15] L. Chrostowski, B. Faraji, W. Hofmann, M.-C. Amann, S. Wieczorek, and W. W. Chow, "40 GHz bandwidth and 64 GHz resonance frequency in injection-locked 1.55 μm VCSELs," *IEEE J. Sel. Topics Quantum Electron.*, vol. 13, no. 5, pp. 1200–1208, Sep./Oct. 2007.

[16] A. Gatto, A. Boletti, P. Boffi, and M. Martinelli, "Adjustable-chirp VCSEL-to-VCSEL injection locking for 10-Gb/s transmission at 1.55 μm," *Opt. Exp.*, vol. 17, no. 24, pp. 21748–21753, Nov. 2009.

[17] K. Hasebe and F. Koyama, "Modeling of all-optical-signal processing devices based on two-mode injection-locked vertical-cavity surface-emitting laser," *Jpn. J. Appl. Phys.*, vol. 45, no. 8B, pp. 6697–6703, Aug. 2006.

[18] H. Kawaguchi, Y. Yamayoshi, and K. Tamura, "All-optical format conversion using an ultrafast polarizationbistable vertical-cavity surface-emitting laser," in *Tech. Dig. Conf. Lasers Electro-Opt.(CLEO)*, 2000, pp. 379–380.

[19] K. H. Jeong, K. H. Kim, S. H. Lee, M. H. Lee, B. S. Yoo, and K. A. Shore, "Optical injection-induced polarization switching dynamics in 1.5 μm wavelength single-mode vertical-cavity surface-emitting lasers," *IEEE Photon. Technol. Lett.*, vol. 20, no. 9–12, pp. 779–781, May/Jun. 2008.

[20] C. C. Lin, H. C. Kuo, P. C. Peng, and G. R. Lin, "Chirp and error rate analyses of an optical-injection gain-switching VCSEL based all-optical NRZ-to-PRZ converter," *Opt. Exp.*, vol. 16, no. 7, pp. 4838–4847, Mar. 2008.

[21] C. H. Chang, L. Chrostowski, and C. J. Chang-Hasnain, "Injection locking of VCSEL," *IEEE J. Sel. Topics Quantum Electron.*, vol. 9, no. 5, pp. 1386–1393, Sep. 2003.

[22] B. Zhang, X. Zhao, D. Parekh, Y. Yue, W. Hofmann, M. C. Amann, C. J. Chang-Hasnain, and A. E. Willner, "Reconfigurable multifunctional operation using optical injection-locked vertical-cavity surface-emitting lasers," *J. Lightwave Technol.*, vol. 27, no. 15, pp. 2958–2963, Aug. 2009.

[23] T. C. Lu, J. Y. Tsai, H. C. Kuo, and S. C. Wang, "Comparisons of InP/InGaAlAs and InAlAs/InGaAlAs distributed Bragg reflectors grown by metalorganic chemical vapor deposition," *Mater. Sci. Eng. B*, vol. 107, no. 1, pp. 66–70, Apr. 2004.

[24] J. H. Shin, B. S. Yoo, W. S. Han, O. K. Kwon, Y. G. Ju, and J. H. Lee, "CW operation and threshold characteristics of all-monolithic InAlGaAs 1.55- μm VCSELs grown by MOCVD," *IEEE Photon. Technol. Lett.*, vol. 14, no. 8, pp. 1031–1033, Aug. 2002.

[25] E. K. Lau, L. J. Wong, and M. C. Wu, "Enhanced modulation characteristics of optical injection-locked lasers: A tutorial," *IEEE J. Sel. Topics Quantum Electron.*, vol. 15, no. 3, pp. 618–633, May/Jun. 2009.

[26] K. Petermann, *Laser Diode Modulation and Noise*. : Taipei, Taiwan: Taipei Publications Trading Company, 1992, ch. 7.

[27] A. Murakami, K. Kawashima, and K. Atsuki, "Cavity resonance shift and bandwidth enhancement in semiconductor lasers with strong light injection ," *IEEE J. Quantum Electron.*, vol. 39, no. 10, pp. 1196–1204, Oct. 2003.

[28] G. P. Agrawal, *Fiber-Optic Communication Systems*. New York: Wiley, 1992, ch. 6.

Chia-Chi Lin received the B.S. degree in materials engineering from Tatung University, Taipei, Taiwan, in 2004, and the M.S. degree in photonics and optoelectronics from the National Taiwan University, Taipei, in 2008.

She is currently at the National Taiwan University, where she is engaged in the study of the laser-diode-based all-optical data format conversion techniques and their application in fiber-optic communication networks. She has authored or coauthored journal and conference papers related to the vertical-cavity surface-emitting laser (VCSEL)-based optical nonreturn-to-zero (NRZ) to return-to-zero (RZ) data format converters.

Yu-Chieh Chi was born in Taipei, Taiwan, in 1983. He received the B.S. degree in electrical engineering and the M.S. degree in electro-optical engineering from the National Taipei University of Technology (NTUT), Taipei, Taiwan, in 2005 and 2007, respectively. He is currently working toward the Ph.D. degree at the Graduate Institute of Photonics and Optoelectronics, National Taiwan University (NTU), Taipei.

He has authored or (co)authored more than ten papers in international periodicals and more than seven papers in international conferences. His current research interests include fiber-optic communications, all-optical data processing, and optoelectronic oscillators.

Hao-Chung Kuo (S'98–M'99–SM'06) received the B.S. degree in physics from the National Taiwan University, Taipei, Taiwan, in 1990, the M.S. degree in electrical and computer engineering from Rutgers University, Camden, NJ, in 1995, and the Ph.D. degree in electrical and computer engineering from the University of Illinois at Urbana-Champaign, Urbana, in 1999.

He has an extensive professional career both in research and industrial research institutions, which includes as follows: Research Consultant with Lucent Technologies, Bell Lab, Holmdel, NJ (from 1995 to 1997), R&D Engineer with the Fiber-optics Division, Agilent Technologies (from 1999 to 2001), and R&D Manager with LuxNet Corporation (from 2001 to 2002). Since September 2002, he has been a Member of the faculty in the Institute of Electro-Optical Engineering, National Chiao Tung University, Hsinchu, Taiwan. He has authored or coauthored more than 60 publications. His current research interests include the epitaxy, design, fabrication, and measurement of high-speed InP- and GaAs-based vertical-cavity surface-emitting lasers, as well as GaN-based lighting-emitting devices and nanostructures.

Peng-Chun Peng (M'10) received the Ph.D. degree from the Institute of Electro-Optical Engineering, National Chiao Tung University, Hsinchu, Taiwan, in 2005.

From 2006 to 2008, he was an Assistant Professor in the Department of Applied Materials and Optoelectronic Engineering and the Department of Electrical Engineering, National Chi Nan University, Taiwan. In 2008, he joined the Department of Electro-Optical Engineering, National Taipei University of Technology, Taipei, Taiwan, as an Assistant Professor. His current research interests include optical communication systems, vertical-cavity surface-emitting lasers, fiber sensors, optical signal processing, and microwave photonics.

Connie J. Chang-Hasnain (M'88–SM'92–F'98) received the B.S. degree from the University of California, Davis, in 1982, and the M.S. and Ph.D. degrees in electrical engineering from the University of California, Berkeley, in 1984 and 1987, respectively.

From 1987 to 1992, she was a Member of Technical Staff at Bellcore. From 1992 to 1995, she was an Associate Professor of electrical engineering at Stanford University, Stanford, CA. Since 1996, she has been a Professor of electrical engineering with the University of California, Berkeley, where she is the John R. Whinnery Chair Professor and the Chair of the Nanoscale Science and Engineering Graduate Group. She is also the Director of the Center for Optoelectronic Nanostructured Semiconductor Technologies. Her current research interests include nanomaterials and optoelectronic devices, and their applications.

Dr. Chang-Hasnain was the recipient of the 1994 IEEE LEOS Distinguished Lecturer Award, the 2000 Curtis W. McGraw Research Award from the American Society of Engineering Education, the 2003 IEEE William Streifer Scientific Achievement Award, and the 2005 Gilbreth Lecturer Award from the National Academy of Engineering. She is a Fellow of the Optical Society of America and the Institution of Electrical Engineers. She has been an Honorary Member of A. F. Ioffe Institute since 2005. She was named a Presidential Faculty Fellow, a National Young Investigator, a Packard Fellow, a Sloan Research Fellow, and the Outstanding Young Electrical Engineer of the Year by Eta Kappa Nu.

Gong-Ru Lin (S'93–M'96–SM'04) received the B.S. degree in physics from Soochow University, Taipei, Taiwan, in 1990, and the M.S. and Ph.D. degrees in electro-optical engineering from the National Chiao Tung University, Hsinchu, Taiwan, in 1990 and 1996, respectively.

He was the Faculty Member of several universities in Taiwan from 1997 to 2006. Since 2006, he has been a Full Professor in the Graduate Institute of Photonics and Optoelectronics (GIPO) and the Department of Electrical Engineering, National Taiwan University (NTU), Taipei, where he is currently directing the Laboratory of Fiber Laser Communications and Si Nano-Photonics in GIPO. He is currently the Deputy Chair of GIPO in NTU and the Chair of the IEEE/Photonics Taipei Chapter. He has authored or coauthored more than 150 SCI-ranked journal papers and 200 international conference papers during his research career. His current research interests include the fiber-optic communications, the all-optical data processing, the femtosecond fiber lasers, the nanocrystallite Si photonics, the ultrafast photoconductors, and the optoelectronic phase-locked loops.

Dr. Lin is a Member of the Optical Society of America (OSA), a Fellow of the International Society for Optical Engineers (SPIE) since 2008, a Fellow of the Institute of Engineering and Technology (IET) since 2009, and a Fellow of the Institute of Physics (IOP) since 2010.